Cr/SiO$_2$ mesoporous catalysts: Effect of hydrothermal treatment and calcination temperature on the structure and catalytic activity in the gas phase dehydration and dehydrogenation of cyclohexanol

Pablo M. Cuesta Zapata [a], Marcelo S. Nazzaro [b], Elio E. Gonzo [c], Mónica L. Parentis [c], Norberto A. Bonini [a],*

[a] INIQUI, CIUNSa, Fac de Ciencias Exactas, Avda. Bolivia 5150, 4400, Salta, Argentina
[b] INFAP, CONICET, Departamento de Física, Avda. Ejercito de los Andes 950, 5700 San Luis, Argentina
[c] INIQUI, CIUNSa, Fac. de Ingeniería, Avda. Bolivia 5150, 4400 Salta, Argentina

ARTICLE INFO

ABSTRACT

Cr/SiO$_2$ mesoporous materials (Cr-MCM-41) were obtained by hydrothermal synthesis. The effect of hydrothermal treatment and calcination temperature on the structure and catalytic behavior of synthesized materials were analyzed. The materials were characterized by XRD, N$_2$ adsorption–desorption, TEM-SEM, TG-DTA, FTIR-HATR, DRUV–vis and XPS. The hydrothermal treatment promoted the incorporation of Cr^{3+} into the silica network, improving their resistance to oxidation. The calcination in air produces the simultaneous presence of Cr^{3+} and Cr^{6+} ions, and their relative amounts depend both on the hydrothermal pretreatment and the calcination temperatures. The Cr^{3+} ions constituted coordinative unsaturated acid centers responsible of the cyclohexanol to cyclohexene dehydration reaction. Moreover, the Cr^{6+} ions correspond to either isolated monochromate species linked to the silica structure or to polychromate aggregates, which produce crystalline α-Cr$_2$O$_3$ clusters after calcination in air to 450 °C. The monochromate centers were active for the dehydrogenation reaction. So, although dehydration was the main reaction, the dehydrogenation reaction to cyclohexanone also was observed after calcination in air to 450 °C.

© 2015 Elsevier B.V. All rights reserved.

1. Introduction

Molecular sieves family, M41S, developed by "Mobil" in 1992, attracted considerable attention due to its high specific surface area, ordered porous structure, and narrow porous size distribution [1–4]. However, this material presents low stability at pH values (pH > 9), which limited its application in basics aqueous systems. Due to this disadvantage, numerous efforts were made to improve its stability by changing the synthesis procedure or by post-synthesis steps modifications. One of the procedures that give better results was the restructuring hydrothermal treatment proposed by Mokaya et al. [5].

The transition metals incorporation into these molecular sieves was deeply studied for their use as heterogeneous catalysts in selective oxidation reactions on various substrates. Chromium is particularly attractive owing to its redox properties and it has a wide application to different oxidation catalytic reactions [6–13]. The strong chromium attachment, to the support preserving the mesoporous structure, is the biggest goal to achieve active catalysts for environmentally friendly oxidation reactions both in liquid and gas phase.

The chromium species dispersion and their redox properties are also crucial factors to obtain highly active catalysts. For this reason the oxidation state and coordination, either as supported chromium oxide or as isolated chromium ion attached to the mesoporous material's surface, has been deeply studied in the bibliography by diverse techniques [14–18]. In this regard, over the Cr/SiO$_2$ "Phillips" catalyst, responsible for more than one third of all the polyethylene (PE) produced in the world, highly extended characterization studies were carried out [18–20]. These studies have proved the presence of chromium in diverse oxidation states (Cr^{2+}, Cr^{3+}, Cr^{5+}, Cr^{6+}) and also the existence of monomeric, dimeric or polymeric oxidized species; the last ones leading to the formation of amorphous or crystalline aggregates. These studies correlated

* Corresponding author. Tel.: +54 387 4251006; fax: +54 387 4251006.
E-mail addresses: pcuesta@unsa.edu.ar (P.M. Cuesta Zapata),
nazzaro@unsl.edu.ar (M.S. Nazzaro), gonzo@unsa.edu.ar (E.E. Gonzo),
mparentis@unsa.edu.ar (M.L. Parentis), bonini@exa.unsa.edu.ar (N.A. Bonini).

the catalytic behavior with the coordination and the oxidation state of the supported chromium species.

Usually, "direct synthesis" methods such as sol–gel, precipitation-deposition and carbonate deposition by one side, or the incipient wetness impregnation by the other, were the most used techniques for the deposition of metallic ions in the matrix of these porous materials and/or for the formation of polymeric superficial oxidized species, respectively. Meanwhile, ion exchange or gas phase deposition methods allow obtaining monodisperse ionic surface species in different coordination states.

The Cr^{n+} incorporation into the structure of the mesoporous molecular sieves with high specific surface area (S_{BET}) is a good strategy to improve the catalytic properties of these materials by developing high dispersion and/or reaching appropriated coordination states of the metallic ion interacting with the support. The conditions during the hydrothermal synthesis, when templates are mixed with Cr^{3+} salt solutions, make possible to generate Cr/SiO_2 materials in which the mesoporous MCM-41 structure prevails with a good catalytic performance.

In a previous work [21], using cetyltrimethylammonium bromide (CTAB) as template and after hydrothermal treatments to different temperatures, Cr-MCM-41 catalysts were obtained with diverse Si/Cr molecular ratio. The hydrothermal treatment up to 150 °C incorporates Cr^{n+} species to the silica structure, preserving the MCM-41 mesoporous structure.

In this work, Cr/SiO_2 (MCM-41) catalysts were synthesized under different hydrothermal conditions. They were obtained through the incorporation of the metallic precursor "in situ", before the hydrolysis and condensation of the silica precursor (TEOS) in the presence of CTAB as template. After the hydrothermal treatment, the materials were heated to 500 °C in N_2 and calcined in air to 300 °C to eliminate the template. The influence of the hydrotreating temperature over the mesoporous structure and the Cr oxidation state was systematically analyzed, and correlated with the catalytic activity in the cyclohexanol reactions. The variation of these properties with the calcination temperature in air between 300 and 450 °C was also analyzed.

2. Experimental

2.1. Sample preparation

2.1.1. Reactants

Tetraethylorthosilicate (TEOS) (Merck >98%) as silica source; cetyltrimethylammonium bromide (CTAB) (Fluka) as surfactant; $Cr(NO_3)_3 \cdot 9H_2O$ (Anedra > 98%) as chromium source; tetramethylammonium hydroxide (TMAOH) (Merck – 20% aqueous solution), ethanol (EtOH) (Merck – 99.9%), and distilled water, were used for the samples synthesis.

2.1.2. Procedure

About 15 g of CTAB dissolved in 137 mL of water was added to a mixture of 38 mL of TEOS, 137 mL of distilled water, and 180 mL of EtOH under vigorous stirring for 30 min at room temperature (RT). Then, 4.1 g of $Cr(NO_3)_3 \cdot 9H_2O$ dissolved in 100 mL of a H_2O:EtOH (1/1) solution was slowly added to the previous mixture, which was stirred for 90 min. The obtained solution was heated up to 50 °C and 20 mL of TMAOH 25% was added. The molar composition of the final mixture was 1.0 TEOS:0.24 CTAB:105 H_2O:25 EtOH:0.25 TMAOH:0.06 Cr. The mixture was allowed to gel during 24 h. Portions of the gel were placed in a Teflon vessel and hydrothermally treated at temperatures between 150 and 220 °C. The obtained solid was filtered and washed with water and EtOH/acetone (1:1) mixture to remove the free chromium. The solid sample obtained was dried at 110 °C, calcined in a nitrogen flow at 550 °C for 19 h and

finally treated in air flow at 300 °C for 3 h to remove the surfactant. The elimination of the surfactant in the sample was monitored by FTIR spectroscopy. The materials were assigned as $5ME_{xxx}^{yyy}$ where xxx is the hydrotreatment temperature and yyy the calcination temperature in air. The non-hydrotreated sample was denoted as $5ME_{nHT}$.

2.2. Sample characterization

2.2.1. Textural characterization

Adsorption–desorption isotherms were carried out in a Micromeritics ASAP-2020 sorptometer, employing N_2 as adsorbate. Specific surface area (S_{BET}) was determined using the standard BET method. The pore size distributions were calculated from the adsorption–desorption isotherms data, using the BJH method.

2.2.2. X-ray diffraction (DRX)

Crystallographic studies and the mesoporous array of the samples were carried out in a RIGAKU-DENKI D-Max IIC powder diffractometer with a 40 V Cu-Kα emission source.

2.2.3. Transmission electron microscopy (TEM)

TEM images were obtained on a JEOL 100CX instrument at an acceleration voltage of 100 kV.

2.2.4. Scanning electron microscopy (SEM)

SEM images were obtained on a JEOL JSM – 6480 LV instrument operating at 15 kV. The samples were previously covered with a thin graphite film.

2.2.5. Thermo-gravimetric (TG) and differential thermal analysis (DTA)

The analysis was carried out in air, in a RIGAKU unit, at a heating rate of 10 °C/min, from room temperature to 1000 °C. The amount of sample used was 15 mg.

2.2.6. Fourier transform infrared spectroscopy (FTIR)

The FTIR spectra were recorded on a Spectrum GX-FTIR Perkin Elmer spectrophotometer. Transmission spectra were obtained from the samples diluted with KBr and pressed at 2 Tn/cm². The spectra were normalized with respect to the height of the band in the 1150–1000 cm^{-1} spectral region.

2.2.7. Horizontal attenuated total reflection (HATR)

HATR-FTIR spectra were recorded on a Spectrum GX-FTIR Perkin Elmer spectrophotometer fitted with a ZnSe horizontal ATR cell, after 10 scans at 4 cm^{-1} resolution.

2.2.8. UV–vis diffuse reflectance spectroscopy (DRUV–vis)

These analyses were carried out in GBC-918 spectrophotometer fitted with a diffuse reflectance sphere, employing $BaSO_4$ as reference. In the 190–900 nm range, spectra were determined from previously ground samples.

2.2.9. X-ray photoelectron spectroscopy (XPS)

The study was performed in situ using a VG Microtech ESCA spectrometer with a non-monochromatic Al Kα radiation (300 W, 15 kV, $h\nu$ = 1486.6 eV) as the excitation source combined with a VG-100-AX hemispherical analyzer operating at 25 eV pass energy. The instrumental resolution was 0.1 eV. The Si2p peak at 103.4 eV was taken as reference for the binding energy (BE) calibration. Samples were outgassed, at room temperature in the preparation chamber (10^{-6} Torr) until constant pressure was achieved, and then introduced to the analysis chamber (10^{-9} Torr) for recording.
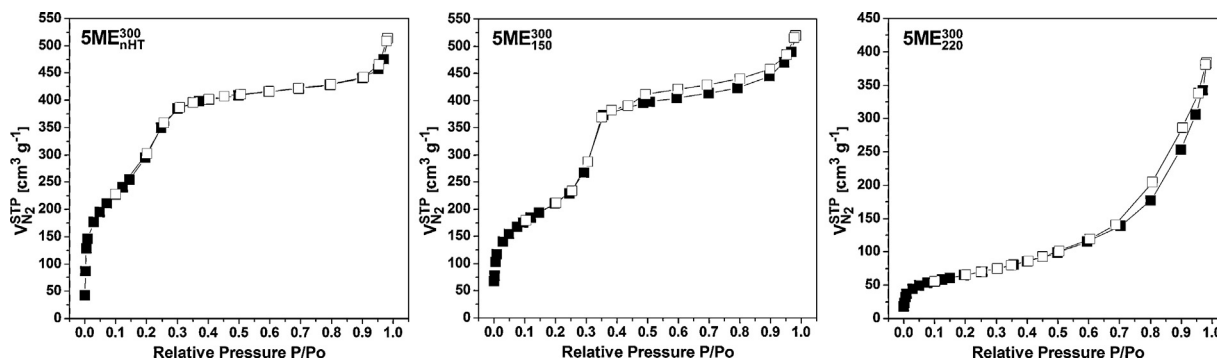
Fig. 1. N_2 adsorption–desorption isotherms (77 K).
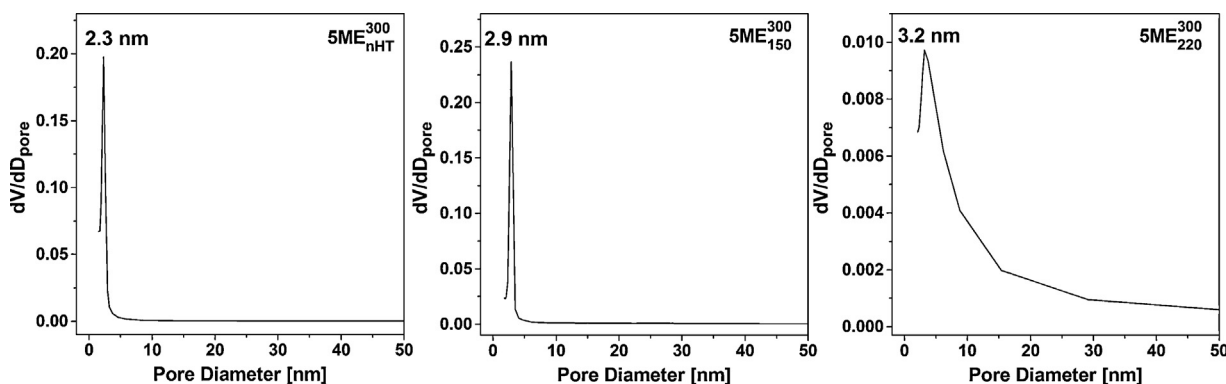
Fig. 2. Mean pore size distribution D_p.

2.2.10. Atomic absorption spectroscopy (AAS)

The sample chromium loading was determined by Atomic Absorption Spectroscopy (AAS), with a GBC 904 AA Spectrometer, after dissolving the samples with HF.

2.3. Catalytic activity

The catalytic activity for the cyclohexanol (CyOH) reaction was carried out at atmospheric pressure in a Pyrex tubular gas flow reactor (internal diameter = 5 mm). The amount of catalyst varied from 50 to 100 mg (80–100 mesh). N_2 and N_2/O_2 mixtures were used as the carrier gas at a flow rate of 180 mL/min. The CyOH was vaporized into the carrier gas to obtain a partial pressure of 0.012 atm. The effluent gas composition was determined by a Shimatzu GC-3B gas chromatograph, fitted with a thermal conductivity detector, over a Carbowax 20M/Chromosorb PAW column.

3. Results and discussion

3.1. N_2 adsorption–desorption isotherms (77 K)

Fig. 1 shows the N_2 adsorption–desorption isotherms of the synthesized samples. The sample without hydrothermal treatment, $5ME_{nHT}^{300}$, and the one treated at 150 °C, $5ME_{150}^{300}$, show type IV isotherms, characteristic of mesoporous solids according to the IUPAC classification [22]. Besides, the $5ME_{150}^{300}$ sample presents a type H4 hysteresis loop characteristic of solids with interparticles pores [22]. On the other hand, the sample hydrothermally treated at 220 °C, $5ME_{220}^{300}$, developed a Type II isotherm, characteristic of open surface solids, with a Type H3 hysteresis loop, inherent to solids formed by particle aggregation [22].

Table 1 summarizes the textural properties, such as S_{BET}, pore volume (V_{STP}) and average pore diameter (D_p), of the 5ME materials

obtained after different hydrotreatments. This table shows that the S_{BET} decreases from 1344 m^2 g^{-1} to 776 m^2 g^{-1} as the temperature of the hydrothermal treatment increases from RT to 150 °C. The abrupt S_{BET} decrease observed in the $5ME_{220}^{300}$ sample reflects the collapse of the ordered mesoporous structure as will be established below.

It can be observed in Fig. 1 that for $P/P_0 < 0.1$, a strong increase of the adsorbed volume (V_{STP}) is produced as a consequence of the N_2 monolayer-multilayer adsorption on the mesopores wall. At higher values of P/P_0, the isotherms show an inflection resembling capillary condensation inside the primary uniform mesopores. This inflection point, moves to higher P/P_0 values as the hydrothermal treatment temperature increases. This shift is a consequence of the pores diameter increase (D_{pores}) (Fig. 2) [4,5,23].

The material without hydrotreatment shows a unimodal distribution centered at Dp = 2.3 nm. This unimodal distribution is conserved by the material treated at 150 °C, but centered at Dp = 2.9 nm. Meanwhile, the material submitted to hydrothermal treatment at 220 °C, presents a wide pore size distribution (maximum at 3.2 nm) characteristic of a SiO$_2$ amorphous material; with a negligible contribution of ordered mesopores as a consequence of the collapse of the structure.

Moreover, the chromium loading (Table 1), in all materials, was lower than the theoretical amount added because the non-anchored chromium was released by washing before drying (see experimental section). Accordingly, the amount of chromium was 30% lesser into the $5ME_{nHT}$ material and 20% lower in the hydrotreated samples. This difference is attributed to the lower amount of water and superficial hydroxyl groups present on the hydrotreated materials (Table 2) as result of the S_{BET} decrease. Though, it must be also consider that, under hydrothermal condition, a certain solubility of the Si-oligomers may occur, leading to a consequent increase in the final chromium amount.

Table 1
Textural properties of prepared materials.

Sample	d_{100} (nm)	S_{BET} (m^2 g^{-1})	V_{STP} (cm^3 g^{-1})	D_p (nm)	a_0 (nm)	t (nm)	%Cr (w/w)
5ME$_{nHT}$^{300}	3.8	1344	0.779	2.3	4.3	2.0	3.5
5ME$_{150}$^{300}	4.3	776	0.796	2.9	5.0	2.1	4.0
5ME$_{220}$^{300}	–	237	0.579	3.2	–	–	4.0

Table 2
Experimental data obtained from TG-DTA thermograms of 5ME materials.

Sample	% total loss of weight	% loss of weight (RT–150 °C)	% loss of weight (150–450 °C)	% loss of weight (450–750 °C)	% loss of weight (750–1000 °C)	T1
5ME$_{nHT}$^{300}	26.5	20.5	2.5	2.5	1.0	306
5ME$_{150}$^{300}	18.0	9.5	4.0	3.5	1.0	313
5ME$_{220}$^{300}	10.5	5.0	3.0	2.0	0.5	325
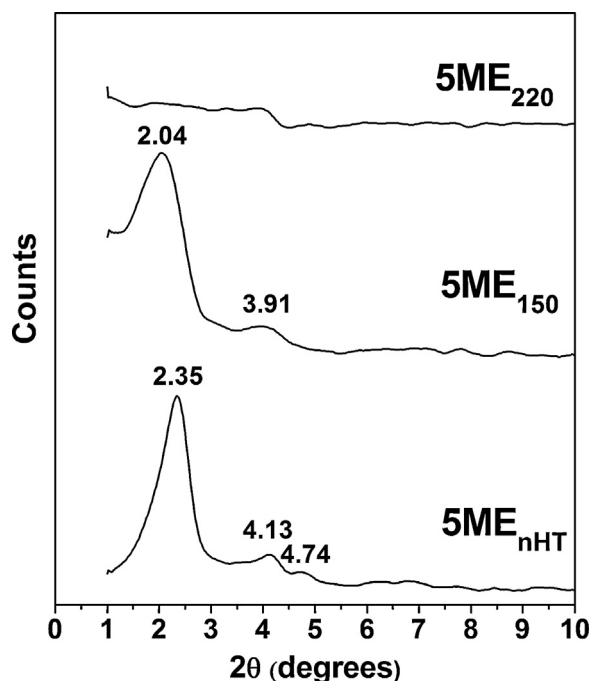
Fig. 3. XRD patterns of samples obtained by different hydrothermal treatments.

3.2. X-ray diffraction studies

Fig. 3 shows the XRD patterns, at low diffraction angles, of the synthesized materials at different hydrothermal treatment temperatures.

In the sample without hydrothermal treatment, 5ME$_{nHT}$, diffraction lines are observed at 2.35, 4.13 and 4.74, units of 2θ. These signals correspond to the hkl diffraction planes (1 0 0), (1 1 0) and (2 0 0), respectively, of a MCM-41 material, with a hexagonal well-ordered structure [2,3].

The diffractogram of the 5ME$_{150}$ sample shows the disappearance of the signal corresponding to the (2 0 0) diffraction plane and an intensity decrease and broadening of the other signals, with displacements to lower 2θ values. These modifications in the diffractogram reflect a diminution in the order of the mesoporous structure and a change in the a_0 cell parameter, as a consequence of the increase of Dp. Both structural parameters relate to the wall thickness between pores through the expression:

$$a_0 = D_p + t$$

where the cell parameter a_0 can be determined from the diffractogram ($a_0 = 2d_{100}/\sqrt{3}$) and D_p is the mean pore diameter calculated by BJH [1,5].

The structural parameters presented in Table 1 show that the hydrothermal treatment up to 150 °C increases the values of the cell parameter a_0, D_p and t respect to those observed in 5ME$_{nHT}$^{300}. Moreover, the samples treated at 220 °C, 5ME$_{220}$, do not present signals at low values of 2θ, revealing the collapse of the ordered mesoporous structure. This behavior is coincident with the low values show of S_{BET} (Table 1), the widening of the pore size distribution (Fig. 2c) and the development of an adsorption isotherm typical from open structure solids (Fig. 1c).

Table 1 also shows the chromium loading in the different synthesized materials. It can be observed a difference between the theoretical chromium content, originally added to the gel (see Section 2.1.2 experimental section), and that experimentally found.

Around 80% of the added chromium was incorporated into the support during the hydrotreatment, while the remaining 20% was eliminated in the different washing steps. A similar behavior was previously observed in amorphous materials of Cr/SiO$_2$ prepared by hydrotreating [24]. Moreover, the increment of the amount of metal incorporated in the samples, when the hydrothermal treatment temperature increases, is attributed to a reduction of the water content as a consequence of the specific surface area decrease confirmed by TG-DTA (see below). Furthermore, diffractograms of the samples, in the 10–80 2θ units range, showed only the typical behavior of amorphous siliceous materials demonstrating the absence of crystalline oxide species.

3.2.1. Transmission electron microscopy (TEM) and scanning electron microscopy (SEM)

Fig. 4 shows electron micrographs obtained by TEM and SEM of the 5ME materials. The TEM micrographs, both in the sample without hydrothermal treatment, 5ME$_{nHT}$^{300} (Fig. 4a) as the sample treated at 150 °C, 5ME$_{150}$^{300} (Fig. 4b), show the existence of a hexagonal uniform mesopores arrangement. Conversely, in the 5ME$_{220}$^{300} sample it is not observed a regular pattern system; which coincides with that found by N$_2$ adsorption and DRX, previously discussed. None of the samples show aggregates of surface chromium oxides.

The scanning electron micrograph (SEM) of the 5ME$_{nHT}$^{300} sample (Fig. 4a), shows spherical particles with a size distribution between 100 and 500 nm, with a high proportion in the 100–250 nm range. In agreement with that reported by Leboda et al. [25], the hydrothermal treatment at 150 °C (Fig. 4b) produces the aggregation of the small diameter particles giving bigger spherical aggregates; remaining only a low amount of small isolated particles. The agglomeration between small particles to form aggregates justifies the Type IV hysteresis loop observed in the

TEM

SEM
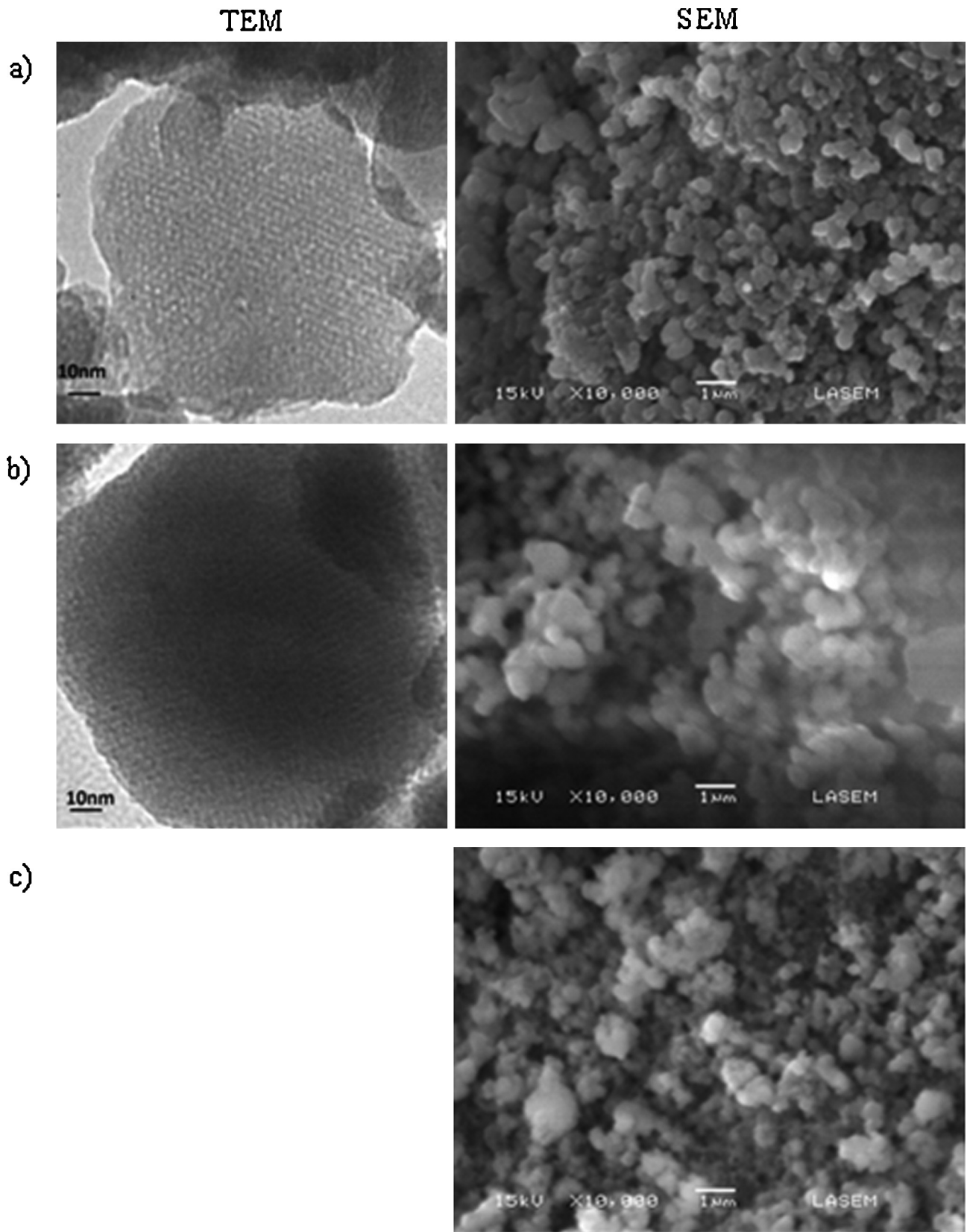
Fig. 4. TEM and SEM micrographs of samples calcined at 300 °C. (a) TEM and SEM 5ME$_{nHT}$^{300}, (b) TEM and SEM 5ME$_{150}$^{300} and (c) SEM5ME$_{220}$^{300}.

adsorption–desorption isotherms (Fig. 1b), characteristic of materials with inter-particles pores.

Finally, the hydrotreatment at 220 °C (Fig. 4c), produces an increase in the particle aggregation and a deformation of the spherical ones, giving a spongy appearance material [25]. This justifies the Type III hysteresis loop observed in the adsorption–desorption isotherms shown in Fig. 1c.
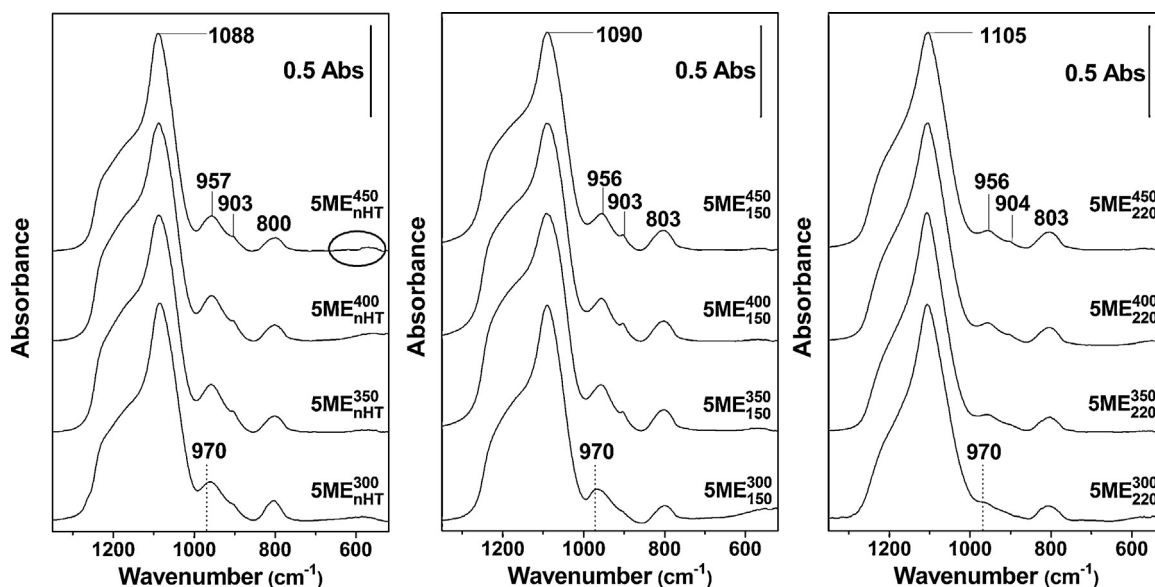
Fig. 5. FTIR spectra of 5ME, structural modification in function of hydrotreatment and calcination temperature.

3.2.2. FTIR and HATR-FTIR study

Fig. 5 shows the transmission FTIR spectra, in the 1350–500 cm^{-1} spectral region, of materials obtained by different hydrothermal treatments and calcined in air between 300 and 450 °C. In this FTIR spectral region, the amorphous silica spectrum shows the presence of three characteristic absorption bands: (a) a wide and high intensity band at 1100 cm^{-1}, with a shoulder around 1200 cm^{-1}, assigned to the asymmetrical stretching (ν_{as}) of the Si—O—Si bonds; (b) a less intense band at 800 cm^{-1} corresponding to the symmetric stretching (ν_s) of the Si—O—Si bonds, and (c) a low intensity one, arising from the stretching of the Si—OH bonds [26].

The replacement by metallic ions of the hydrogen atoms of superficial Si—OH groups causes a diminution of the intensity of the third band and their shift to lower frequencies. The magnitude of the shift depends on the chemical characteristics of the metal used. In the case of Cr^{3+} ion, a band assigned to Si—OCr bond stretching was observed at 970 cm^{-1} [6,24]. So, the decrease in the intensity of this band as the temperature of the hydrothermal treatment increases, is related both to the drop of the S_{BET} and the incorporation of the Cr^{+3} ions into the silica structure.

In materials calcined in air, bands at 903 and 956 cm^{-1} are observed. These bands, assigned to the ν_s and ν_{as} vibrations of the O=Cr=O bonds, respectively, are characteristic both of oxidized isolated Cr^{6+} species and polychromate compounds [6,27]. Their intensity increases as the calcination in air temperature goes from 300 to 450 °C for a given hydro treatment temperature. However, as the temperature of hydrotreatment increases, the intensity of these bands increases more slowly. Accordingly, in the 5ME$_{220}$ (Fig. 5c) materials the intensity of the 903 and 956 cm^{-1} bands are low, even after calcination on air at 450 °C. However, they are already observed in the 5ME$_{nHT}$^{300} spectrum (Fig. 5a). This material without hydrothermal treatment (Fig. 5a), calcined in air at 450 °C is the only one who, besides the previous bands indicated, presents a couple of very weak bands at 564 and 619 cm^{-1}. These new bands are characteristic of the ν_s and ν_{as} vibrations of the O—Cr—O bonds of α-Cr$_2$O$_3$ formed from polychromate clusters [28]. This behavior reflects an increase in the support metal interaction and a high oxidation resistance of the isolated Cr^{3+} incorporated into the silica structure as a consequence of the hydrotreatment.

The amorphous silica structure can be described by the presence of different oligomeric species Q_n, where n ($0 \leq n \leq 4$),

represents the number of next-nearest neighboring Si atoms. Among these oligomers is possible to differentiate those who form the internal polymer structure (Q_{nint}) and those finishing the three-dimensional net (Q_{next}). The existence and the amount of each type of oligomers can be determinates by ^{29}Si NMR or FTIR spectroscopy. Zholobenko et al. [29], demonstrated that the Q_{3int} oligomers (ν_{as} 1040–1060 cm^{-1}) are the most abundant in the MCM-41 wet materials, and that its amount decreases as result of further condensation forming Q_{4int} oligomer units (ν_{as} 1100–1120 cm^{-1}), after the material is dried or calcined. The Q_{4ext} and Q_{3ext} oligomer units present adsorption bands at 1220 and 1180 cm^{-1}, due to the ν_{as} of the bonds in the (SiO)$_3$SiOH and (SiO$_4$) tetrahedral, respectively. The bandwidth (HWTM) corresponding to ν_{as} (Si—O—Si), located at 1100 cm^{-1} approximately, reflects the Si—O—Si bonds heterogeneity. The hydrothermal treatment produces a band shift from 1088 cm^{-1} (5ME$_{nHT}$^{300}) to 1105 cm^{-1} (5ME$_{220}$^{300}), and a lower HWTM in agreement with previously pointed out. Furthermore, it can be observed, at 1220 cm^{-1}, a band shoulder decrease due to the partial disappearance of Q_{4ext} units (1220 cm^{-1}) and to the Q_{3ext} formation. It can be concluded that the increase of hydrothermal treatment temperature leads to amorphous SiO$_2$ materials formation with a much more uniform structure. On the other hand, from the spectra in Fig. 5, it can be observed that the hydrothermal treatment has a higher influence than the calcinations treatment, on the silica structure.

3.3. Horizontal attenuated total reflection (HATR)

To understand the structural changes observed in the obtained materials after different hydrothermal treatment, FTIR spectroscopic analysis was made using the HATR technique. Since in the HATR technique the light penetrates only a few micrometers in the sample, optically dense samples such as aqueous solutions can be very well studied. However, the spectra reflect mainly the composition of the solution, but not the dispersed solid [30].

Fig. 6a illustrates the spectra corresponding to aqueous dispersions of the gel materials (5ME) submitted to different hydrothermal treatments after water washes to eliminate the surfactant residues remaining in solution. In all the spectra is observed two signals at 1045 and 1086 cm^{-1}, corresponding to the presence of the same oligomer soluble precursor, independently of the thermal treatment to which the mixture was submitted.
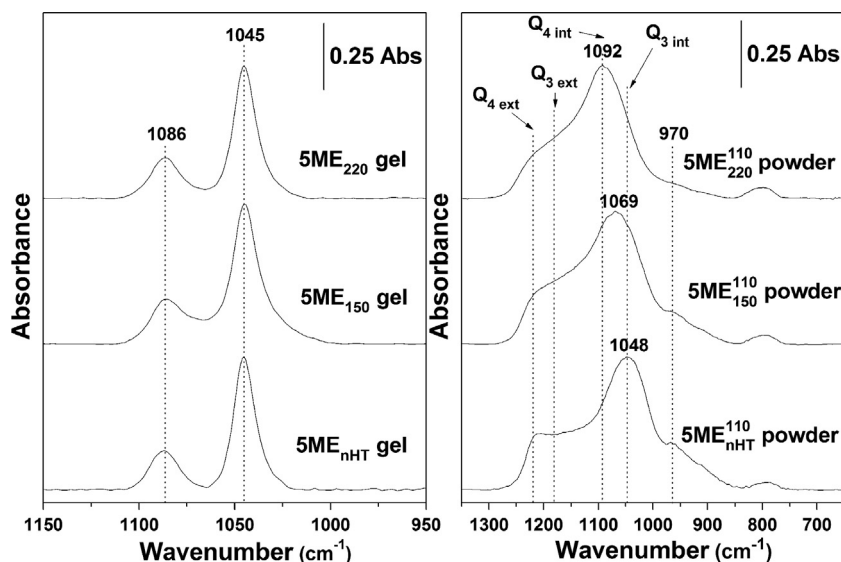
Fig. 6. HATR spectra of 5ME catalysts (a) in gel forms as synthesized at different hydrotreatments, (b) in air at 110 °C.

Fig. 6b shows the HATR spectra of samples dried at 110 °C. It can be observed that the hydrothermal treatment effect on the silica structure is not the same for the different materials. The samples without hydrotreatment present two adsorption bands with maximum at 1048 and 1210 cm^{-1}. As the temperature of the hydrothermal treatment increases, a shift of the first signal to higher frequencies and of the second to lower frequencies occurs.

This shift is related to the formation of Q_{4int} instead of Q_{3int} oligomer species, whose signal disappears as the samples are submitted to more severe hydrothermal treatments. From the profile of the spectra in the region between 1250 and 1150 cm^{-1} is possible to have an approximation of the concentration ratio between the different oligomers in the external gel structure; since the Q_{3ext} oligomers present a band at 1180 cm^{-1}, while Q_{4ext} oligomers species present a band at 1220 cm^{-1} [29]. Looking at the spectra, it can be concluded that the sample without hydrothermal treatment shows a higher concentration of $Q_{4extern}$ species respect to the $Q_{nextern}$ ($n < 4$); which is deduced from the intensity of the shoulder at 1220 cm^{-1}. As consequence of the hydrothermal treatment, there is an increase of the external oligomer species of low order ($n < 4$), mainly of the type Q_{3ext}, which leads to a band intensity loss at 1220 cm^{-1}.

Therefore, it can be concluded that by effect of the hydrothermal treatment there is an increase in the "internal" Q_{4int} respect to the "external" Q_{4ext} oligomer species, which agrees with the results obtained by transmission FTIR (Fig. 5).

3.3.1. Thermal analysis TG-DTA

The results obtained by TG-DTA of the samples calcined in air at 300 °C and submitted to different hydrothermal treatments (5ME$_{nHT}$^{300}, 5ME$_{150}$^{300} and 5ME$_{220}$^{300}), are shown in Fig. 7.

Between approximately 20 and 150 °C, an endothermic band accompanied by an important loss of weight attributed to the elimination of physically adsorbed and occluded water, is observed in all the samples. At temperatures higher than 150 °C, a continuous loss of weight is produced as a consequence of different dehydration processes [31,32]. Table 2 shows the total weight loss (%) and the loss of weight corresponding to different temperature ranges. Up to 150 °C the physisorbed water is totally lost, while between 150 and 450 °C the loss of weight is due to the water elimination by condensation of vicinal silanol groups. Between 450 and 750 °C is produced the geminal silanols condensation and finally, between 750 and 1000 °C, occurs the elimination of remaining

isolated silanols groups and the silica sintering. The total weight loss and the endothermic band intensity until 190 °C are directly related to the change in the S_{BET} and the surface hydroxylation degree.

In the sample without hydrothermal treatment (5ME$_{nHT}$^{300}), as well as on samples treated hydrothermally at 150 °C, the area of the endothermic peak and the total weight loss are proportional to its S_{BET} (Table 1). Above 150 °C, the hydrotreatment increases the density of Q_{3ext} oligomers promoting a relatively higher loss of water by condensation of silanol groups.

All the 5ME materials developed, besides the endothermic band from the progressive water elimination, an exothermic peak in the range between 300 and 325 °C. With the hydrotreating temperature increase, the maximum of this peak (Fig. 7 and Table 2) shifts to higher values while increases their area. This peak is assigned to the oxidation of Cr^{3+} to Cr^{6+}, attached to the surface by SiO-Cr bonds. These chromium species remain as Cr^{+3} after calcination in air at 300 °C. Their amount and resistance to oxidation increase with the rise of the hydro treating temperature, consequence of a higher metal–support interaction [33,34].

3.3.2. Diffuse reflectance spectroscopy (DRS UV–visible)

Fig. 8 presents the DRSUV–vis spectra displayed by samples prepared at different hydrotreatment temperatures and submitted to calcination in air between 300 and 400 °C.

The 5ME$_{nHT}$^{300} catalyst spectrum (Fig. 8a) presents four absorption bands at 270, 355, 445 and 665 nm. The bands at 270 and 355 nm correspond to charge-transfer transitions from ligand to metal (LMCT)(O→Cr(VI)) in chromate type species with the metal in tetrahedral coordination [14,15]. The band at 445 nm is a complex band arising from the d–d transition ($^4T_{1g}(F) \rightarrow {}^4T_{2g}(F)$), characteristic of Cr(III) species in octahedral coordination and the LMCT O→Cr^{6+}(1t$_1$→2e) transition prohibited by symmetry. In spite of being a prohibited transition, the last band increases its intensity in di or polychromate species, being its contribution more important than the correspondent to the d–d ($^4T_{1g}(F) \rightarrow {}^4T_{2g}(F)$) transition [14,15]. Finally, the band at 665 nm, assigned to the d–d ($^4T_{2g}(F) \rightarrow {}^4A_{2g}(F)$) transition, is characteristic of Cr^{3+} species whose octahedral coordination gets distorted as they are incorporated into the support [13,24].

The rise of the calcination temperature increases the intensity of the signals corresponding to Cr(VI) species, both as chromates or as di or polychromates, while the bands corresponding to Cr(III)
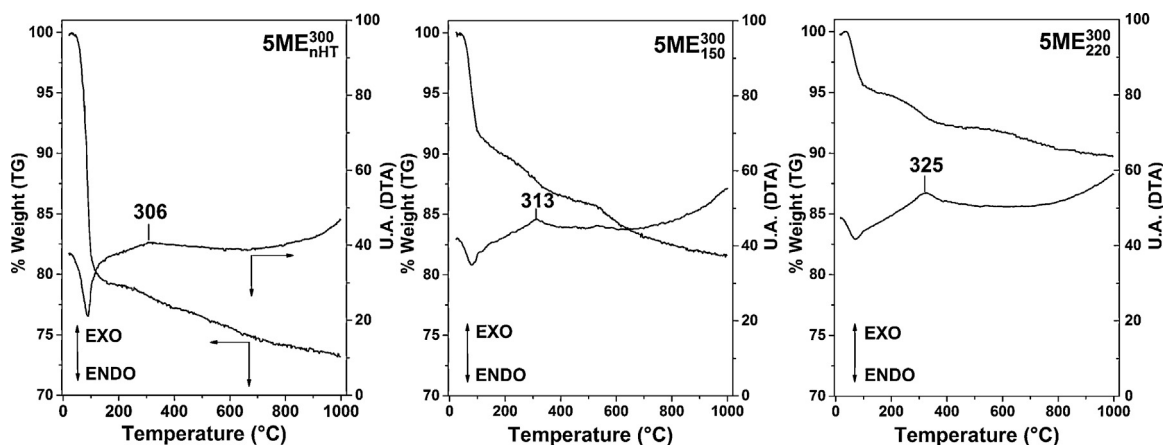
Fig. 7. TG-DTA of 5ME materials calcined in air at 300 °C. (a) $5ME_{nHT}^{300}$, (b) $5ME_{150}^{300}$ and (c) $5ME_{220}^{300}$.
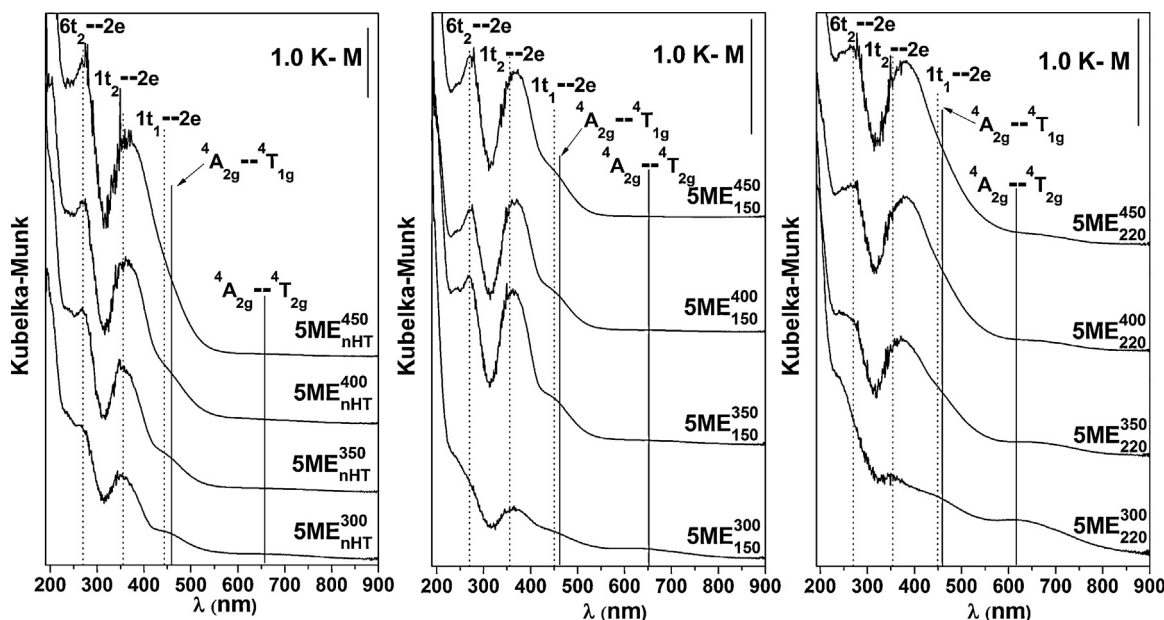
Fig. 8. DRUV–vis spectra of mesostructurated samples as a function of calcination temperature. (a) $5ME_{nHT}$, (b) $5ME_{150}$ and (c) $5ME_{220}$.

decrease. Accordingly, the spectrum of the sample calcined at 450 °C ($5ME_{nHT}^{450}$) shows mainly the bands at 260 and 355 nm while those at 445 and 665 nm practically disappear. The disappearance of the signal at 445 nm is associated with an important widening in the 355 nm band. This is related to the presence of α-Cr_2O_3, previously observed by FTIR (Fig. 5a) and XRD (Fig. 11), which is formed from segregated species of polychromates.

The spectrum of $5ME_{220}^{300}$ sample clearly shows the bands, at 445 nm and 665 nm, corresponding to Cr(III) species. On this material, only weak signals, characteristic of Cr(VI), at 270 and 355 nm are observed. The rise in the calcination temperature leads to a gradual intensification of the last one and a diminution of the signals corresponding to Cr(III) species. In the $5ME_{220}^{450}$ spectrum (Fig. 8c) the Cr^{+3} signal is observed at 665 nm, besides the characteristic signals corresponding to Cr(VI) species, even though the signal at 445 nm has gone.

The samples with hydrotreatment at 150 °C (Fig. 8b) present an intermediate behavior between the observed on samples without HT and those treated at 220 °C.

The DRUV–vis spectra of the samples calcined at different temperatures provide evidence about the increasing effect of the metal support interaction and on the Cr^{3+} oxidation resistance as a consequence of hydrothermal treatment. So, while, on $5ME_{nHT}^{350}$ the Cr(III) bands are weakly developed, on $5ME_{220}^{450}$ the Cr^{3+} signals are notoriously observed together with the Cr^{6+} bands. Another important fact is the diminution of the polychromates/chromate ratio in hydrothermally treated materials, due to their high resistance to segregate oxides, despite the S_{BET} decrease.

3.3.3. X-ray photoelectron spectroscopy (XPS)

Fig. 9 shows the XPS spectra, obtained on samples submitted to hydrothermal treatments and calcined in air at different temperatures. The increment of the XPS signal intensity, as the temperature of the hydrothermal treatment increase (Fig. 9), suggests that in the samples with highly ordered porous structure, the greater amount of chromium is on the internal pore surface where it is not detected by the XPS technique. As the hydrotreatment temperature rise and the mesoporous structure disappear, the signal intensity increase due to that great part of chromium get exposed in the "XPS accessible" external surface of the catalyst.

On the spectra of the calcined samples is observed the simultaneous presence of signals of Cr^{3+} (577 eV) and Cr^{6+} (579 eV), whose relative intensity are modified by the calcination temperature. At the same time a shift to higher binding energy (BE) values
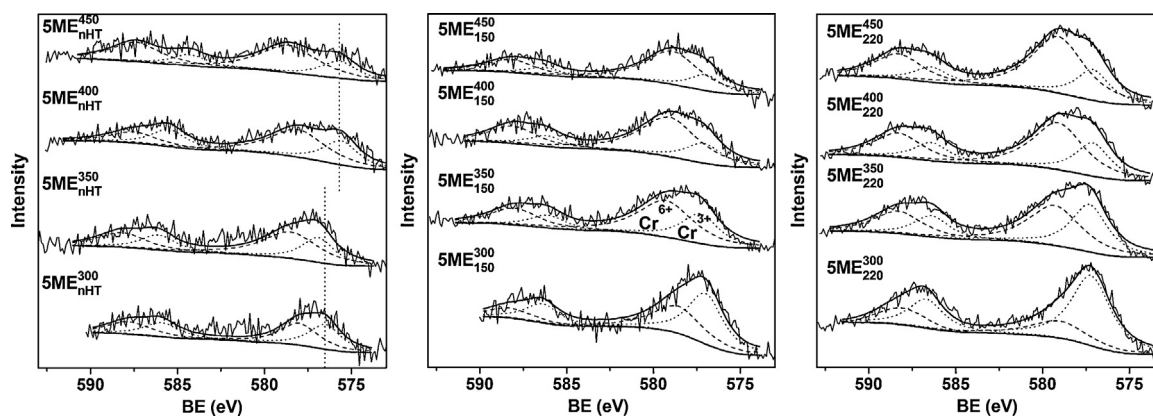
Fig. 9. Cr2p XPS spectra of mesostructurated samples as a function of calcination temperature. (a) $5ME_{nHT}$, (b) $5ME_{150}$ and (c) $5ME_{220}$.

Table 3
BE and FWHM variation in function of hydrothermal treatment.

Sample	Oxidation state assignment	Cr2p(3/2)	
		BE (eV)	FWHM
$5ME_{nHT}{}^{300}$	3+	576.5	2.2
	6+	578.0	2.7
$5ME_{150}{}^{300}$	3+	577.0	2.4
	6+	578.6	3.4
$5ME_{220}{}^{300}$	3+	577.2	2.7
	6+	579.0	3.8

is produced as the hydrothermal treatment temperature increases (Table 3) [16,17].

Table 3 displays the BE and FWHM values of samples calcined at 300 °C. The $5ME_{nHT}{}^{300}$ sample presents signals at 576.5 and 578 eV for Cr^{3+} and Cr^{6+}, respectively; while the $5ME_{220}{}^{300}$ spectrum develops BE values at 577.2 and 579.0 eV. This shift to higher BE values is related to an increase in the metal support interaction by formation of Si—O—Cr bonds, improving the oxidation resistance.

The XPS spectra deconvolution allows the calculation of the relative amount of the Cr^{3+} and Cr^{6+} species present in the different materials. Fig. 10 shows the variation of the $(Cr^{3+}/Cr^{3+} + Cr^{6+})$ ratio with hydrothermal treatment and calcination temperature. In this figure, it can be observed that in calcined samples at 300 °C, the Cr^{3+} content increases as the hydrothermal treatment increases.

The rise in the calcination temperature leads to the diminution of Cr^{3+} content due to the oxidation to Cr^{6+}. However, the oxidation to Cr^{6+} is lower in samples with hydrotreatment at high temperatures.
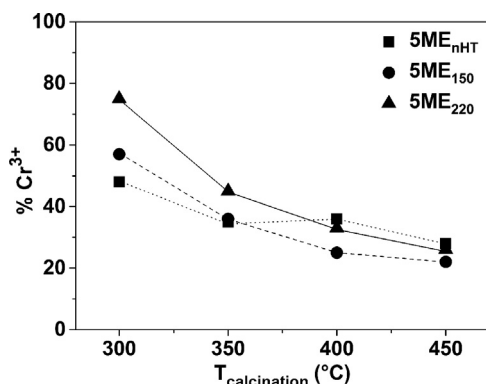
Fig. 10. Relative amount $(Cr^{3+}/Cr^{3+} + Cr^{6+})$ variation in function of calcination temperature in 5ME materials with different hydrotreatments.
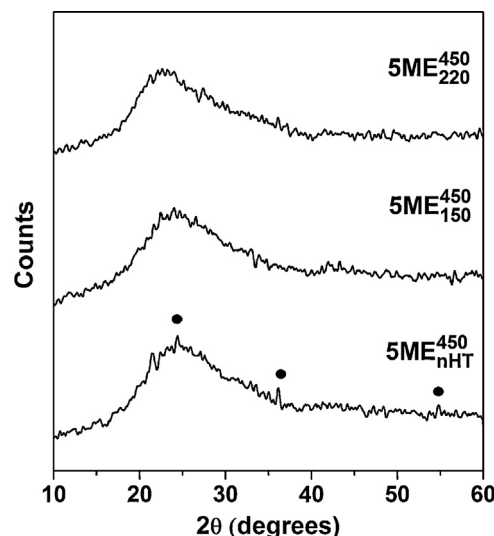
Fig. 11. DRX patterns of materials with different thermal hydrotreatments calcined in air at 450 °C.

Moreover, on the $5ME_{nHT}$ samples is observed, at 400 °C, an increase of the relative Cr^{3+} amount, which is accompanied by a BE diminution (Fig. 9a).

This behavior coincides with the α-Cr_2O_3 signals appear in the XRD of the sample calcined at 450 °C (Fig. 11), as a consequence of the oxygen lost by calcination of the segregated Cr^{6+} oxides. This sample shows weak signals at $2\theta = 24.5°$, 36.2° and 54.8°, characteristic of the presence of α-Cr_2O_3 (JCPDS N° 84-1616) [35].

The α-Cr_2O_3 formation was only observed in the sample without hydrothermal treatment after in air calcination to 450 °C. In this sample, the low metal–support interaction lets the segregation of the Cr^{+6} oxides. This agrees with the XPS spectra (Fig. 9) of the other samples hydrothermally treated at different temperatures and calcined in air at 450 °C. Therefore, the samples treated hydrothermally at 150 and 220 °C ($5ME_{150}{}^{450}$ and $5ME_{220}{}^{450}$), do not present in their XRD pattern signals corresponding to the formation of chromium crystalline species (Fig. 11).

3.3.4. Catalytic activity

The gas phase cyclohexanol reaction over supported catalysts goes through different mechanisms according to the catalyst characteristics. So, on strongly acid catalysts the dehydration reaction to form cyclohexane is the predominant, but the dehydrogenation/oxy-dehydrogenation or oxidative decomposition reactions to form cyclohexanone or CO_2 are very noticeable
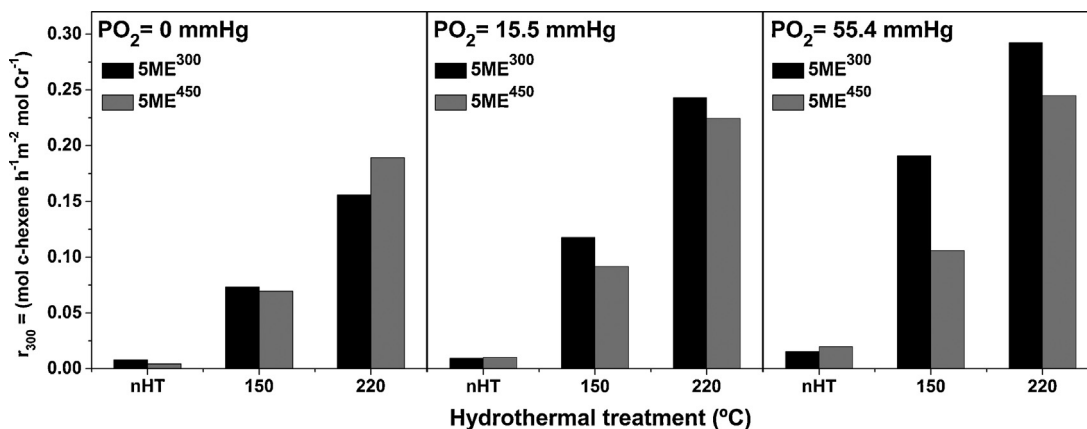
Fig. 12. Dehydration rate at 300 °C in function of hydrothermal treatment and calcination temperature, for different O_2 pressures.
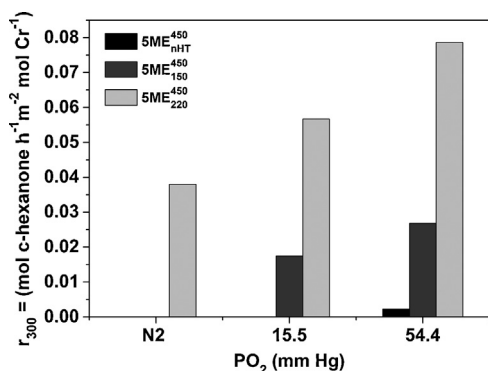
Fig. 13. Cyclohexanone production rate (300 °C) in function of hydrothermal treatment and calcination temperature, for different O_2 pressures.

when catalysts have redox superficial centers. On the Cr/SiO_2 catalysts, the relative amount of these products depends on the metal–support interaction developed by the hydrothermal treatment and calcination temperature.

The catalytic behavior in the gas phase cyclohexanol reaction of the different catalysts prepared, are represented in Figs. 12–14. Fig. 12 shows the dehydration reaction rate at 300 °C, measured at different oxygen partial pressures. This figure also shows the effect of the calcination temperature on samples submitted to different hydrothermal treatments. The materials calcined at 300 °C (5ME^{300}) show only dehydrating activity, independently from the hydrotreatment temperature or oxygen partial pressure employed. This dehydrating activity increases with the rise of the hydrothermal treatment temperature. So, the sample without
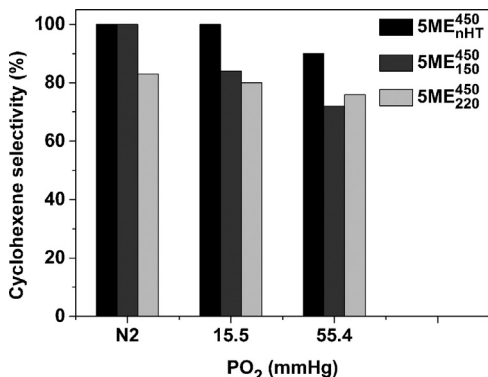
Fig. 14. Cyclohexene selectivity variation with the O_2 pressure in materials calcined in air at 450 °C.

hydrotreatment (5ME$_{nHT}$^{300}) shows a dehydration rate almost an order of magnitude lower than the observed in the sample prepared at 150 °C (5ME$_{150}$^{300}). This behavior reflects the increment of the catalyst acidity as a consequence of the hydrotreatment.

According to the results obtained by characterization techniques, it was concluded that the hydrothermal treatment leads to the incorporation of Cr^{3+} ions to the support structure, which is reflected by the BE values (Fig. 9, Table 3) corresponding to the Cr2p(3/2) peaks. This incorporation produces the formation of chromasiloxanes cycles [18,20,36], in which the angular tension and the coordinative unsaturation of the Cr^{3+}ions increase with the hydrothermal treatment temperature [18,20,36]. In a previous work [24], the presence of these centers was related to the dehydrating activity of these materials.

The increase of the oxygen pressure in the reaction atmosphere did not modify significantly neither the reaction rate nor the selectivity, which remained at 100% to the alkene formation.

It can be observed (Fig. 12) that the calcination in air at 450 °C of the materials submitted to hydrotreatment leads to a diminution of its dehydrating activity as a consequence of the partial oxidation of the Cr^{3+} to Cr^{6+} centers. Over these materials, the increase in oxygen pressure leads to an increase in the reaction rate to the cyclohexanone formation (Fig. 13), due to the presence of the Cr^{6+} centers. Fig. 13 presents the dehydrogenation rate on 5ME catalysts obtained by different hydrothermal treatments calcined in air at 450 °C and at different oxygen partial pressures. In the absence of oxygen, the catalyst treated hydrothermically at 220 °C, 5ME$_{220}$^{450}, has only dehydrating activity. The catalyst prepared at 150 °C, 5ME$_{150}$^{450}, presents dehydrogenating activity from oxygen partial pressures of 15.5 mm Hg, while the material without hydrothermal treatment presents oxy-dehydrogenating activity at oxygen partial pressures of 54.4 mm Hg. In all cases, the dehydrogenation activity was much lower than the dehydration, which is reflected in the high alkenes selectivity values, which was always greater than 70% (Fig. 14).

Fig. 14 shows the selectivity to cyclohexene as a function of the oxygen partial pressure on catalysts calcined at 450 °C. These catalysts produce the highest conversion to cyclohexanone due to the high Cr^{6+} sites concentration. The increment of oxygen partial pressure leads to an increase of the dehydrogenation reaction rate (Fig. 13). The materials 5ME$_{nHT}$^{450} and 5ME$_{150}$^{450}, which in N_2 present only dehydrating activity, in the presence of oxygen (54.4 mmHg) led to the cyclohexanone formation with selectivities between 10% and 28%, respectively.

As discussed previously, the dehydrogenating activity is related to the presence of Cr^{6+} sites, generated from the oxidation of Cr^{3+} species in strong interaction with the support do to the chromasiloxanes formation. On the other hand, those Cr^{6+} ions weakly

linked to the support, that form polychromates precursors by oxidation, have little or null dehydrogenating activity. They tend to transform to α-Cr$_2$O$_3$ by the effect of the calcination in air at 450 °C.

4. Conclusions

Cr/SiO$_2$ catalysts were prepared by the sol–gel method where the chromium salt and the surfactant (CTAB) were added prior to hydrolysis and condensation of the silica precursor (TEOS). This synthesis method allowed obtaining highly ordered mesoporous materials (Cr-MCM-41), with a very narrow pore size distribution. The ordered mesoporous structure, with slight deformation, was maintained up to a hydrotreatment temperature of 150 °C. The hydrothermal treatment at 220 °C produced the collapse of the ordered mesostructure and the formation of an amorphous Cr-SiO$_2$ material.

The surfactant removal required a treatment in N$_2$ at 550 °C and the subsequent calcination in air at 300 °C. The materials calcined at this temperature present the chromium species as Cr^{3+} and Cr^{6+}. The Cr^{3+} ions are present in a distorted octahedral coordination, incorporated into the silica structure. The Cr^{6+} ions with tetrahedral coordination correspond to isolated monochromate species linked to the silica structure and to polychromate aggregates that produce crystalline α-Cr$_2$O$_3$ clusters after calcination in air to 450 °C.

The hydrothermal treatment increases the incorporation of Cr^{3+} into the support, improving their resistance to oxidation. This Cr^{+3} ions constitute coordinative unsaturated acid centers responsible of the cyclohexanol to cyclohexene reaction. Although dehydration was the main reaction, after calcination in air up to 450 °C, cyclohexanone also was observed.

References

[1] J.S. Beck, J.C. Vartuli, W.J. Roth, M.E. Leonowicz, C.T. Kresge, K.D. Schmitt, C.T.W. Chu, D.H. Olson, E.W. Sheppard, J. Am. Chem. Soc. 114 (1992) 10834.
[2] C.T. Kresge, M.E. Leonowicz, W.J. Roth, J.C. Vartuli, J.S. Beck, Nature 359 (1992) 710.
[3] T.J. Barton, L.M. Bull, W.G. Klemperer, D.A. Loy, B. McEnaney, M. Misono, P.A. Monson, G. Pez, G.W. Scherer, J.C. Vartuli, O.M. Yaghi, Chem. Mater. 11 (1999) 2633.
[4] X.S. Zhao, G.Q. Lu, G.J. Millar, Ind. Eng. Chem. Res. 35 (1996) 2075.
[5] R. Mokaya, W. Zhou, W. Jones, J. Mater. Chem. 10 (2000) 1139.
[6] M.L. Parentis, N.A. Bonini, E.E. Gonzo, Latin Am. Appl. Res. 32 (2002) 41.
[7] M.L. Parentis, N.A. Bonini, E.E. Gonzo, React. Kinet. Catal. Lett. 72 (2001) 303.
[8] M. Gruttadauria, L.F. Liotta, G. Deganello, R. Noto, Tetrahedron 59 (2003) 4997.
[9] L.F. Liotta, A.M. Venezia, G. Pantaleo, G. Deganello, M. Gruttadauria, R. Noto, Catal. Today 91–92 (2004) 231.
[10] S. Kawi, M. Te, Catal. Today 44 (1998) 101.
[11] S.K. Mohapatra, P. Selvam, J. Catal. 249 (2007) 394.
[12] U. Schuchardt, D. Cardoso, R. Sercheli, R. Pereira, R.S. da Cruz, M.C. Guerreiro, D. Mandelli, E.V. Spinacé, E.L. Pires, Appl. Catal. A: Gen. 211 (2001) 1.
[13] A. Sakthivel, S.E. Dapurkar, P. Selvam, Appl. Catal. A: Gen. 246 (2003) 283.
[14] A. Bensalem, B.M. Weckhuysen, R.A. Schoonheydt, J. Phys. Chem. B 101 (1997) 2824.
[15] B.M. Weckhuysen, A.A. Verberckmoes, A.R.D. Baets, R.A. Schoonheydt, J. Catal. 166 (1997) 160.
[16] B. Liu, P. Šindelář, Y. Fang, K. Hasebe, M. Terano, J. Mol. Catal. A: Chem. 238 (2005) 142.
[17] A.B. Gaspar, C.A.C. Perez, L.C. Dieguez, Appl. Surf. Sci. 252 (2005) 939.
[18] E. Groppo, C. Lamberti, S. Bordiga, G. Spoto, A. Zecchina, Chem. Rev. 105 (2005) 115.
[19] M.P. McDaniel, in: C.G. Bruce, K. Helmut (Eds.), Advances in Catalysis, vol. 53, Academic Press, 2010, p. 123.
[20] A. Zecchina, E. Groppo, A. Damin, C. Prestipino, in: C. Copéret, B. Chaudret (Eds.), Surface and Interfacial Organometallic Chemistry and Catalysis, vol. 16, Springer, Berlin/Heidelberg, 2005, p. 1.
[21] P.M. Cuesta Zapata, M.S. Nazzarro, M.L. Parentis, E.E. Gonzo, N.A. Bonini, Chem. Eng. Sci. 101 (2013) 374.
[22] K.S.W. Sing, D.H. Everett, R.A.W. Haul, L. Moscou, R.A. Pierotti, J. Rouquérol, T. Siemieniewska, Pure Appl. Chem. 57 (1985) 603.
[23] H. Schmidt, H. Böttner, The Colloid Chemistry of Silica, vol. 234, American Chemical Society, 1994, pp. 419.
[24] P.M. Cuesta Zapata, M.L. Parentis, E.E. Gonzo, N.A. Bonini, Appl. Catal. A: Gen. 457 (2013) 26.
[25] R. Leboda, E. Mendyk, A. Gierak, V.A. Tertykh, Colloids Surf A: Physicochem. Eng. Aspects 105 (1995) 181.
[26] G. Ricchiardi, A. Damin, S. Bordiga, C. Lamberti, G. Spanò, F. Rivetti, A. Zecchina, J. Am. Chem. Soc. 123 (2001) 11409.
[27] K.-T. Li, W.-T. Weng, J. Taiwan Inst. Chem. Eng. 40 (2009) 48.
[28] M.I. Zaki, N.E. Fouad, Thermochim. Acta 95 (1985) 73.
[29] V.L. Zholobenko, S.M. Holmes, C.S. Cundy, J. Dwyer, Microporous Mater. 11 (1997) 83.
[30] D.C. Calabro, E.W. Valyocsik, F.X. Ryan, Microporous Mater. 7 (1996) 243.
[31] L.T. Zhuravlev, The Colloid Chemistry of Silica, vol. 234, American Chemical Society, 1994, pp. 629.
[32] H.E. Bergna, The Colloid Chemistry of Silica, vol. 234, American Chemical Society, 1994, pp. 1.
[33] R.B. Fahim, M.I. Zaki, N.E. Fouad, M. Abdel-Khalik, N. Sheppard, Appl. Catal. A: Gen. 265 (2004) 229.
[34] S.A. Halawy, N.E. Fouad, M.A. Mohamed, M.I. Zaki, J. Therm. Anal. Calorim. 65 (2001) 167.
[35] L. Zhang, Y. Zhao, H. Dai, H. He, C.T. Au, Catal. Today 131 (2008) 42.
[36] C.A. Demmelmaier, R.E. White, J.A. van Bokhoven, S.L. Scott, J. Catal. 262 (2009) 44.